Thermofluid dynamics and droplets transport inside a large university classroom: Effects of occupancy rate and volumetric airflow

Journal of Aerosol Science 175 (2024) 106285

Contents lists available at ScienceDirect

Journal of Aerosol Science

journal homepage: www.elsevier.com/locate/jaerosci

Thermofluid dynamics and droplets transport inside a large university classroom: Effects of occupancy rate and volumetric airflow

Andrea Carlo D'Alicandro [a,*], Alfonso Capozzoli [b], Alessandro Mauro [a]

[a] Dipartimento di Ingegneria, Università Degli Studi di Napoli "Parthenope", Centro Direzionale, Isola C4, 80143, Napoli, Italy
[b] Dipartimento Energia "Galileo Ferraris", Politecnico di Torino, TEBE Research Group, BAEDA Lab, Corso Duca Degli Abruzzi 24, Torino, 10129, Italy

ARTICLE INFO

Handling Editor: Chris Hogan

Keywords:
University classroom
Droplet transport
Air Change per Hour (ACH)
Computational Fluid Dynamics (CFD)
Thermal plume
Airborne transmission

ABSTRACT

The airborne droplets released by humans while speaking or coughing are the main sources of human-to-human contagion for airborne transmissible diseases. Due to the recent SARS-Cov2 pandemic, indoor transmission in classrooms and other environments is an interesting topic investigated by the scientific community. In this work, the thermofluid dynamic conditions and the droplet transport was analysed in a large University Classroom (UC), as a function of the inlet airflow and the occupancy rate. These parameters assume a relevant role in the design stage. However, their effects on droplet transport were not deeply investigated in the literature. Therefore, different conditions were analysed, such as: full occupancy, which represents the design condition where no social distancing is enforced; half occupancy, which is representative of social distancing; and empty UC, to be considered as a term of comparison. The main novelty of this work is related to the analysis of the combined effect of thermal plume and airflow in a large UC. The numerical model for the thermofluid dynamics simulation was validated in a previous work and the droplet emission model was retrieved from the literature. High volumetric airflow is not always beneficial for the reduction of the airborne transmission risk. An important aspect is related to the combined effect of the inlet airflow and the thermal plume, which cannot be ignored if the occupancy rate assumes a significant value. Moreover, the evacuation rate and the age of the droplets are relevant indicators to assess the cleaning time.

1. Introduction

The liquid droplets exhaled from the human mouth and nose can carry viruses and bacteria, making human-to-human contagion possible (Balachandar, Zaleski, Soldati, Ahmadi, & Bourouiba, 2020; Xie, Li, Chwang, Ho, & Seto, 2007). Examples of these pathogens are: the SARS-Cov-2 virus, influenza viruses, Mycoplasma pneumonia, group A streptococcus, bacterial meningitis and many others (Chin, 2000; Xie et al., 2007). Airborne transmission is one of the main routes for the transmission of such diseases (Buonanno et al., 2022; Morawska & Cao, 2020).

The diameter of droplets emitted by a person during expiratory activities (i.e. breathing, talking, coughing, sneezing, etc.) is in the range of 0.5–2000 μm (Johnson et al., 2011; Morawska et al., 2009; Nicas, Nazaroff, & Hubbard, 2005). Droplets with a diameter

* Corresponding author.
E-mail address: andreacarlo.dalicandro001@studenti.uniparthenope.it (A.C. D'Alicandro).

https://doi.org/10.1016/j.jaerosci.2023.106285
Received 4 August 2023; Received in revised form 6 October 2023; Accepted 10 October 2023
Available online 14 October 2023

Nomenclature

$C_{1\varepsilon}$ and $C_{2\varepsilon}$ empirical constants
C_D droplet drag coefficient
C_n (part. cm^{-3}) droplet concentration
d_d (μm) or (m) droplet diameter
$d_{post\text{-}ev}$ (μm) post-evaporation droplet diameter
$d_{pre\text{-}ev}$ (μm) pre-evaporation droplet diameter
e (J kg^{-1}) specific total energy
F_D (N) drag force acting on the droplet
F_g (N) gravity force acting on the droplet
I (%) turbulent intensity
k (J kg^{-1}) turbulent kinetic energy
k_{eff} (W m^{-1} K^{-1}) effective thermal conductivity
m_d (kg) droplet mass
p (Pa) pressure
p_{rgh} (Pa) pressure minus the hydrostatic pressure
P_b (J kg^{-1} s^{-1}) generations of turbulence kinetic energy due to buoyancy
P_k (J kg^{-1} s^{-1}) generations of turbulence kinetic energy due to the mean velocity gradients
Re_d droplet Reynolds number
S_k (J kg^{-1} s^{-1}) generic sources terms for the k
S_ε (J kg^{-1} s^{-2}) generic sources terms for the ε
Stk Particle Stokes number
S_H (J s^{-1} m^{-3}) external energy entering the system
T (°C) temperature
t (s) time
u (m s^{-1}) air velocity
u_d (m s^{-1}) droplet velocity
x_d (m) trajectory of the droplet
x (m) length
Y_M (J kg^{-1} s^{-1}) contribution of the fluctuating dilatation in compressible turbulence

Greek symbols
α_t (m^2 s^{-1}) turbulent thermal diffusivity
δ Kronecker delta
ε (J kg^{-1} s^{-1}) turbulent kinetic energy dissipation
μ (Pa s) dynamic viscosity
μ_t (Pa s) turbulent dynamic viscosity
ν_t (m^2 s^{-1}) turbulent kinematic viscosity
ρ (kg m^{-3}) fluid density
ρ_d (kg m^{-3}) or (g cm^{-3}) droplet density
σ_ε turbulent Prandtl number for the ε
σ_k turbulent Prandtl number for the k
$(\tau_{ij})_{eff}$ (N m^{-2}) deviatronic part of the stress tensor
ψ non-volatile percentage composition of the droplet

Subscript
i, j, k dimensional axis versors

Superscript
$\bar{}$ averaged value
‘ turbulent fluctuation

Acronyms
ACH Air Change per Hour
BC Boundary Condition
CFD Computational Fluid Dynamics
GAMG Geometric Algebraic MultiGrid
HVAC Heating Ventilation and Air Conditioning
LPT Lagrangian Particle Tracking
RNG Re-Normalisation Group

RPM	Revolutions Per Minute
UC	University Classroom

larger than 100 μm have a quasi-ballistic trajectory and settle in a distance lower than 2 m from the source, because the gravity force is greater than the aerodynamic force (Cortellessa et al., 2021; Xie et al., 2007). The particle with a diameter between 20 and 100 μm can be suspended in the air for a prolonged time before settling (Arpino, Cortellessa, Grossi, & Nagano, 2022; Xie et al., 2007), due to the balance between the forces acting on the droplet and droplet diameter reduction caused by evaporation (Balachandar et al., 2020). Droplets with a diameter smaller than 20 μm can remain suspended in the air for a very long time (Johnson et al., 2011; Morawska et al., 2009), especially if the motion of air is turbulent, and therefore may increase the risk of disease transmission. University Classrooms (UCs) are one of the most critical indoor environments for infection transmission especially due to the presence of at least one person continuously speaking (the professor) and the high occupancy rate. The assessment of the contagion risk in UCs is not an easy task, because these environments are not standardized in terms of room and Heating Ventilation and Air Conditioning (HVAC) system layout (type, position and number of inlets and outlets, and operating conditions), occupancy rate, the combined effects of natural and mechanical ventilation and relative volumetric airflow and velocity, and other factors (Arpino et al., 2023).

Droplet transport in indoor environments was extensively investigated in recent years, due to the SARS-Cov-2 pandemic; some review works summarize all the progress achieved and the principal results in this field (Cardelli et al., 2022; Ding, Zhang, & Bluyssen, 2022; Guo et al., 2021; Y. Zhang, Hui, Duffield, & Saeed, 2022). From the literature emerges the undisputed primary role of the air distribution pattern as an influencing factor in the airborne transmission of the disease (Abuhegazy, Talaat, Anderoglu, Poroseva, & Talaat, 2020; Cardelli et al., 2022). Although indoor ventilation can reduce the infection risk, it alone cannot prevent indoor airborne transmission. (Y. Zhang et al., 2022). At the same time, there is a lack of knowledge about the design of ventilation systems in terms of air distribution and volumetric flow rates needed to ensure a reasonably safe environment for the occupants of a classroom (Ding et al., 2022). For instance, an Air Change per Hour (ACH) (h^{-1}) of more than 5 h^{-1} in schools and residential rooms could reduce an influenza outbreak at a community level and delay the rise of the epidemic curve with any airborne virus (Gao, Li, & Leung, 2009; Y. Zhang et al., 2022). Instead, the specific ACH value that can completely eliminate the risk of transmission of the airborne particulate matter remains a subject of investigation (Guo et al., 2021), and further studies are needed to determine whether, and in which conditions, airborne droplets can be spread by air and HVAC system in different rooms of the same buildings (Guo et al., 2021).

Computational Fluid Dynamics (CFD) could be a great support for the optimal design of inlet/outlet diffusers and to assess the performance of HVAC systems at part-load conditions in terms of indoor environmental control conditions in classrooms and other indoor spaces (Arpino et al., 2023; Cardelli et al., 2022). CFD allows to numerically simulate different scenarios in a relatively low time and to investigate factors that influence the thermofluid dynamic conditions and mass transport (D'Alicandro & Mauro, 2022; 2023a). There are a lot of works that have numerically studied aerosol transport in indoor environments, the results of some of those works that have analysed classrooms are that ACH is not always an effective solution to improve indoor air quality, because in some cases increasing the ACH can result in a local or global increase of the aerosol concentration. In fact, the airflow patterns should be considered during the design stage of the HVAC systems also considering the risk of exposure to airborne diseases (Arpino et al., 2023). The airflow pattern strongly influences the droplet's motion characterized by a lower diameter, while the droplets with a diameter larger than 45 μm follow the air pattern only for a short distance before falling (Ren, Wang, Liu, & Liu, 2021). This numerical result is coherent with experimental works, even if it is still unclear the diameter limit which allows droplets to stay suspended in a turbulent environment for a prolonged time (Arpino, Cortellessa, et al., 2022; Johnson et al., 2011; Morawska et al., 2009; Xie et al., 2007). A further critical factor in indoor aerosol transport is the distance between the droplet source and the occupants, highlighting the importance of a proper HVAC system design and the choice of optimal operating conditions, such as inlet volumetric airflow and temperature (Foster & Kinzel, 2021). In fact, different ventilation strategies and inlet and outlet positions lead to different zones of higher risk and different values of droplet concentration (Arjmandi, Amini, khani, & Fallahpour, 2022; He, Niu, Gao, Zhu, & Wu, 2011).

Mechanical ventilation could be in some cases coupled with natural ventilation, leading to the so-called mixed ventilation. Natural ventilation effectively reduces air contaminants and improves indoor air quality (Y. Wang et al., 2014), but during the coldest and hottest months of the year, it should be avoided due to the difference between outdoor climatic conditions and the desired indoor thermo-hygrometric set-point (D'Alicandro & Mauro, 2023a; International Organization for Standardization, 2005). Therefore, it is crucial to investigate the effects of the HVAC system on aerosol transport. Moreover, while open windows may help in increasing the ACH, they can also generate problems as the air inflow near the breathing plane carries droplets from a potentially infected person near the window to other occupants (Rencken, Rutherford, Ghanta, Kongoletos, & Glicksman, 2021). An alternative solution to reduce the contagion risk can be the employment of physical partitions (Mirzaie et al., 2021).

Another aspect that needs careful consideration is the heat gains emitted by students in the UC, which can generate the so-called thermal plume. Thermal plume was studied both in classrooms (Rencken et al., 2021; Su et al., 2022) and in other indoor environments with the presence of people (D'Alicandro & Mauro, 2023a; Liu, Yin, et al., 2021a; Yan, Li, & Tu, 2019). In these works, the thermal plume has no negligible effect even if the occupancy rate of the indoor environment is not high. The works that numerically (Arjmandi et al., 2022; Foster & Kinzel, 2021; Rencken et al., 2021; Su et al., 2022) or experimentally (Dacunto, Moser, Ng, & Benson, 2022) studied the thermal plume and/or the droplet transport inside classrooms used a social distancing configuration ($\sim$2 m between the students) and the classroom was for 50 or fewer students.

The novelty of the present work is mainly related to the analysis of the droplets transport in a real large university classroom, as a function of the thermal plume and airflow, for different occupancy rates and inlet conditions. In particular, at full occupancy, the UC

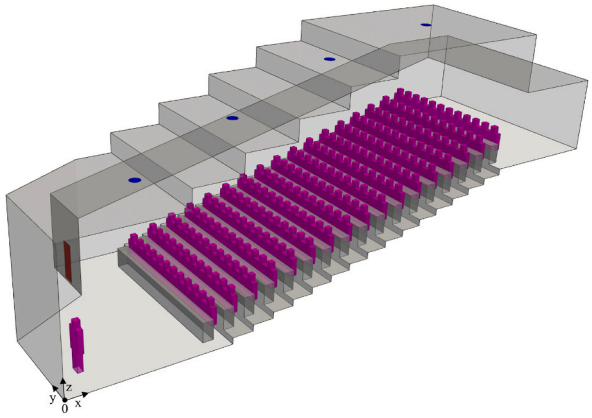

Fig. 1. Layout of the UC 3D domain at full occupancy rate.

can accommodate 408 students, and there is no distance between the people in the same row, providing a consequent significant effect on the thermal plume. Instead, the half occupancy rate condition analysed in this paper is representative of a situation where social distancing is in effect. Moreover, the authors have considered a case with no students in the room, in order to have a term of comparison, to further analyse the effect of the thermal plume and airflow on the droplets transport.

Eventually, it is important to remark that the results of works that investigate a particular case should be interpreted under the context of the HVAC system layout and student occupancy rate assumed in the related models. Other UCs may employ different HVAC systems and may necessitate aerosol transport simulation tailored to the specific UC (Abuhegazy et al., 2020). The HVAC system layout and the droplet source position have a fundamental role in droplet distribution in the UC (Abuhegazy et al., 2020).

Considering the above literature analysis, in order to reduce the gap in the knowledge on the effects of the ACH and thermal plume on droplet transport and thermofluid dynamic conditions inside UCs, the authors have developed a Eulerian-Lagrangian methodology to numerically analyse the variation of the airflow pattern, droplet concentration, deposition, evacuation and age (time that they are suspended in the air) as a function of the ACH (HVAC system operating conditions) and occupancy rate (thermal plume effect). Some authors have validated the thermofluid dynamics model against experimental measurement in a smaller UC equipped with swirl diffusers (D'Alicandro & Mauro, 2023b) and have used the droplet transport model to simulate the droplet transport in a UC (Arpino et al., 2023). The UC considered in the analysis is a real classroom at the Politecnico di Torino (Turin, Italy).

The objectives of the present work can be summarized as follows:

(i) To find the better ACH value, among those analysed, (ii) to weigh the importance of the thermal plume in a large environment characterized by a large number of occupants, taking into account different occupancy rates (full, half and empty), (iii) to analyse the fate of droplets (settled on surfaces, evacuated by the HVAC system, still suspended in the air), their age and spatial distribution, (iv) to find the optimal cleaning time between different lessons, to reduce the cross-contamination and (v) to verify if the use of physical barriers brings advantages in terms of airborne transmission.

The paper is organized as follows. In Section 2 the cases analysed and the UC layout are represented. In Section 3 the numerical methodology developed is described. In Section 4 the results obtained and the factors that influence droplet transport inside the UC are analysed. In section 5 the conclusions are drawn.

2. Case study

In this work, the thermofluid dynamic condition and the droplet transport in a UC within the Politecnico di Torino (Turin, Italy), were numerically analysed as a function of the UC occupancy rate (full, half and empty) and the HVAC system inlet conditions, mainly the volumetric airflow (i.e. the ACH) and the air temperature.

The UC has the following geometrical characteristics: dimensions (respectively x, y, z) of 22.41 m $\times$ 15.90 m x 9.00 m with a floor-ceiling height varying from 3.00 m to 6.10 m and a total gross volume of 1608 m^3, therefore, it can be considered a large classroom. There are 17 desk rows, each of which is split by the central stairs and can accommodate 24 students. The HVAC system installed is a turbulent mixing airflow system. It is equipped with eight swirl diffusers (with a diameter of 0.40 m), divided into two rows and equally distributed on the ceiling, and two extraction grilles (1.40 m $\times$ 0.55 m) at the UC side. The UC presents a symmetry plane in the middle therefore, in order to reduce the computational time, half of UC was simulated. The layout of the UC three-dimensional domain at full occupancy is displayed in Fig. 1. In this figure, the four diffusers are coloured in blue, the extraction grille in red, the humans in purple and the walls in grey, with partial transparency to improve clarity.

To decouple the effects of the HVAC system inlet condition (operating condition) and the thermal plume generated by human heat, the simulations were divided into two groups. In the first group, the UC occupancy rate was maintained at its maximum (408 students) and three different inlet volumetric airflows were simulated: 10,000 $m^3\,h^{-1}$ (equal to 6.22 ACH), that is the design operating condition of the room, and the maximum value used; 8000 $m^3\,h^{-1}$ (equal to 4.98 ACH); 6000 $m^3\,h^{-1}$ (equal to 3.73 ACH). The full occupancy rate is the design condition of the UC. This group of simulations make it possible to study the effects of the inlet airflow, while maintaining

Table 1
Summary of the simulated cases.

Case	Occupancy rate	Inlet volumetric airflow ($m^3\ h^{-1}$); RPM ($min.^{-1}$)	Volumetric airflow per student ($m^3\ h^{-1}\ pers.^{-1}$)	Inlet air temperature (°C)
Case 1: 6000 $m^3\ h^{-1}$, 408 students	Full (408 students)	6000; 60	14.70	15
Case 2: 8000 $m^3\ h^{-1}$, 408 students	Full (408 students)	8000; 80	19.61	15
Case 3: 10,000 $m^3\ h^{-1}$, 408 students	Full (408 students)	10,000; 100	24.51	15
Case 4: 10,000 $m^3\ h^{-1}$, 204 students	Half (204 students)	10,000; 100	49.02	15
Case 5: 10,000 $m^3\ h^{-1}$, 0 students	Empty (0 students)	10,000; 100	n.a.	15

constant occupant heat generation (i.e. the number of students), on the thermofluid dynamic conditions and droplet transport inside the UC.

In the second group of simulations, the occupancy rate was changed from full occupancy to half occupancy (204 students) and to empty (0 students); in that case, the HVAC system inlet conditions were considered equal for all three cases: 10,000 $m^3\ h^{-1}$ (equal to 6.22 ACH). This second group of simulations make it possible to analyse the effects of the thermal plume on the indoor airflow pattern, with the same inlet volumetric airflow. The half occupancy condition can be considered as a condition to ensure social distancing. It was created considering a layout that alternates an occupied seat with a vacant one. In all the simulated cases, the professor is present in the room, because he/she is the droplet source due to speaking. Moreover, the inlet air temperature is equal to 15 °C for all cases.

The ACH was calculated with respect to the gross UC volume (1608 m^3). The swirl diffusers installed in the UC are characterized by a fan rotation varying in the range from 60 to 100 Revolutions Per Minute (RPM) ($min.^{-1}$). All the simulated cases are summarized in Table 1.

The professor is the only person continuously talking during the lesson, therefore he/she was chosen as the unique droplet source. In common practice, the students are supposed to talk occasionally and for a short period, therefore their contribution to droplet emission was considered negligible with respect to that of the teacher. On this basis, the droplet transport simulation was simulated for 1 h (3600 s), which is the typical time of a lecture before having a break or completing the lesson.

The RPM value (Table 1) was used as input value in the inlet boundary condition to calculate the tangential component of the air velocity, coplanar with the boundary surface and perpendicular to the radius. At each point of the inlet, it is the product between the RPM (converted in seconds) and the local length of the radius. Therefore, only the component along the z-axis is uniform, while the component in the x-y plane goes from a value of 0 to RPM•diffuser radius.

3. Methodology

The authors have employed OpenFOAM software to develop the mathematical model and perform both the thermofluid dynamics and droplet transport simulations. The numerical model is based on the finite volume method. First, the steady-state thermofluid dynamics simulation was performed, with a Eulerian approach, to calculate thermal and fluid dynamic fields; then the transient droplet transport simulation was performed with a Lagrangian approach. The droplet transport evolves on the steady-state velocity field calculated in the thermofluid dynamics simulation, ensuring a drastic reduction of the computational load and time required, compared to simulating simultaneously both the air velocity field and droplet transport with a transient approach. The effects of turbulence and thermal plume were taken into account in the thermofluid dynamics simulation to obtain a more realistic velocity field. The hypothesis of both the thermofluid dynamics model and droplet transport model are based on a solid literature base and the OpenFOAM solvers employed are fully validated. The thermofluid dynamics model, i.e., the solver, turbulence model and Boundary Conditions (BCs) employed, was validated against experimental measurements taken in a smaller UC with swirl diffusers (the same diffuser used in the current UC) (D'Alicandro & Mauro, 2023b) and used in two works of some of the authors of the present paper with appropriate modifications according to the HVAC system used (D'Alicandro & Mauro, 2022; 2023a). The adopted droplet emission model was used in a previous work by some of the authors of the present paper (Arpino et al., 2023) and in other literature works (Arpino, Cortellessa, et al., 2022; Arpino, Grossi, et al., 2022; Cortellessa et al., 2021, 2023; S. Xu, Zhang, Liu, & Li, 2023).

3.1. Thermofluid dynamics model

The Reynolds number, calculated at the inlet, is larger than $4{\cdot}10^4$ for all cases, therefore the airflow inside the UC is turbulent. The Re-Normalisation Group (RNG) k-ε was employed to model the turbulence phenomena. The RNG k-ε is a two-equation turbulence model which is coupled with the Reynolds-averaged Navier–Stokes equations (or RANS equations) employed to simulate the turbulent airflow conjugated with the heat transfer. The theory and discretization of the RANS equations and turbulence model can be found in the literature (Pope, 2000; Versteeg & Malalasekera, 2007; Wilcox, 2006). The RANS (equation 1-3) and RNG k-ε (equation 4, 5) equations are reported in a concise way:

$$\frac{\partial \rho}{\partial t} + \frac{\partial (\rho \overline{u}_i)}{\partial x_i} = 0 \tag{1}$$

$$\frac{\partial (\rho \overline{u}_i)}{\partial t} + \frac{\partial \left(\rho \overline{u}_i \overline{u}_j\right)}{\partial x_j} = -\frac{\partial p}{\partial x_i} + \frac{\partial}{\partial x_j}\left[\mu\left(\frac{\partial \overline{u}_i}{\partial x_j} + \frac{\partial \overline{u}_j}{\partial x_i} - \frac{2}{3}\delta_{ij}\frac{\partial \overline{u}_k}{\partial x_k}\right)\right] + \frac{\partial\left(-\rho \overline{u_i' u_j'}\right)}{\partial x_j} \tag{2}$$

$$\frac{\partial (\rho \overline{e})}{\partial t} + \frac{\partial [\overline{u}_i (\rho \overline{e} + \overline{p})]}{\partial x_i} = \frac{\partial}{\partial x_j}\left(k_{eff}\frac{\partial \overline{T}}{\partial x_j} + \overline{u}_i \left(\tau_{ij}\right)_{eff}\right) + S_h \tag{3}$$

$$\frac{\partial \rho k}{\partial t} + \frac{\partial \rho k u_i}{\partial x_i} = \frac{\partial}{\partial x_j}\left[\left(\mu + \frac{\mu_t}{\sigma_k}\right)\frac{\partial k}{\partial x_j}\right] + P_k - \rho\varepsilon \tag{4}$$

$$\frac{\partial \rho \varepsilon}{\partial t} + \frac{\partial \rho \varepsilon u_i}{\partial x_i} = \frac{\partial}{\partial x_j}\left[\left(\mu + \frac{\mu_t}{\sigma_\varepsilon}\right)\frac{\partial \varepsilon}{\partial x_j}\right] + C_{1\varepsilon}\frac{\varepsilon}{k}P_k - C_{2\varepsilon}\rho\frac{\varepsilon^2}{k} \tag{5}$$

Where, for the RANS equation: the subscripts i, j, k represent the dimensional axis versors; the $\overline{\ }$ superscript represents the averaged value; the superscript ‘represents the turbulent fluctuation; x (m) is the length; ρ (kg m^{-3}) is the fluid density; t (s) is the time; p (Pa) is the pressure; μ (Pa s) is the dynamic viscosity; e (J kg^{-1}) is the specific total energy; δ is the Kronecker delta; $(\tau_{ij})_{eff}$ (N m^{-2}) is the deviatronic part of the stress tensor S; k_{eff} (W m^{-1} K^{-1}) is the effective thermal conductivity and S_H (J s^{-1} m^{-3}) is the external energy entering the system. $-\rho\overline{u_i' u_j'}$ (N m^{-2}) is the Reynolds stress tensor, a component of the total stress tensor in turbulent fluid flow. While for the RNG k-ε equations: μ_t (Pa s) is the turbulent dynamic viscosity; σ_ε and σ_k are respectively the turbulent Prandtl number for the ε and the k; P_k and P_b (J kg^{-1} s^{-1}) are respectively the generations of turbulence kinetic energy due to the mean velocity gradients and due to buoyancy; Y_M (J kg^{-1} s^{-1}) is the contribution of the fluctuating dilatation in compressible turbulence; S_k (J kg^{-1} s^{-1}) and S_ε (J kg^{-1} s^{-2}) are respectively the generic sources terms for the k and ε. The empirical constants $C_{1\varepsilon}$ and $C_{2\varepsilon}$, assume different values in the function of the application and fluid flow characteristics.

The RNG version of the k-ε turbulence model was introduced to improve the performance for a specific class of flow (Pope, 2000; Yakhot, Orszag, Thangam, Gatski, & Speziale, 1992). The theoretical model was formulated by Yakhot et al. (Yakhot et al., 1992) and it has proved to have better performance compared to other k-ε models for indoor airflow analysis (Abuhegazy et al., 2020; Chen, 1995; D'Alicandro & Mauro, 2023b; Massarotti, Mauro, Sainas, Marinetti, & Rossetti, 2019; Rohdin & Moshfegh, 2007; Stavrakakis, Koukou, Vrachopoulos, & Markatos, 2008; Tian, Tu, Yeoh, & Yuen, 2006). The RNG k-ε was used to simulate turbulent airflow and aerosol transport in different indoor environments (Abuhegazy et al., 2020; D'Alicandro, Massarotti, & Mauro, 2021; D'Alicandro & Mauro, 2022, 2023a; Isukapalli et al., 2013; Liu, Zhang, et al., 2021b; Mirzaie et al., 2021; Tian et al., 2006; G. Xu & Wang, 2017; Zhao, Zhang, Li, Yang, & Huang, 2004). Therefore, the RNG k-ε model is suitable for thermofluid dynamics and aerosol transport simulation in indoor environments. *buoyantSimpleFoam* is the OpenFOAM solver employed to perform the steady-state thermofluid dynamics simulation. *buoyantSimpleFoam* is a compressible steady-state turbulent solver based on the SIMPLE algorithm (Caretto, Gosman, Patankar, & Spalding, 2007). Due to the low temperature gradient in the UC, the air was considered incompressible and the Boussinesq approximation was employed to calculate the buoyancy force. The effect of the radiative heat transfer on the velocity field was neglected due to the low ratio between emitting surface (humans) and total surface area (Chow, Lin, & Bai, 2006). The surface human temperature was set at an average value of 33 °C (Fiala, Lomas, & Stohrer, 1999; Massarotti, Mauro, Mohamed, Nowak, & Sainas, 2020). There are two reasons why steady-state airflow was preferred to a full transient simulation (both thermofluid dynamics and droplet transport simulations). First, the airflow in a complex ambient like a large UC depends on a lot of factors such as quantity and distribution of persons, HVAC inlet condition, presence of windows, etc. Therefore, the steady-state airflow is representative of the average airflow. The second reason is that simulating the transient droplet transport on an evolving (transient) airflow would have required a computational time much larger, making the simulations unpracticable without a dedicated server.

The size of the mouth, the volume of air exhaled, the respiratory cycle time and the quantity and dimension of droplets emitted vary from person to person and as a function of the indoor conditions and performed activity (Abkarian, Mendez, Xue, Yang, & Stone, 2020; Benchetrit et al., 1989; Gupta, Lin, & Chen, 2009, 2010; Johnson et al., 2011; Kwon et al., 2012; Mahjoub Mohammed Merghani, Sagot, Gehin, Da, & Motzkus, 2021; C. Xu, Nielsen, Liu, Jensen, & Gong, 2017). Therefore, to carry out the present simulations, average values were identified from the literature. The size of the mouth was chosen equal to 5 cm^2 (Abkarian et al., 2020), the mean value of the tidal volume (during the exhalation) is 1 l s^{-1} (Abkarian et al., 2020; Gupta, Lin, & Chen, 2010) and the respiration cycle is 5 s, with an exhalation time between 66% and 80% of the respiration cycle (Abkarian et al., 2020), resulting in a total exhalation airflow between 3.3 and 4 l per respiration cycle. Therefore, to simulate a steady-state airflow, only the exhalation phase was considered with a total tidal volume during the exhalation phase of 3.3 l, resulting in a constant exhalation airflow of 0.66 l s^{-1} (1.32 m s^{-1}), used as a boundary condition. The choice of simulating a steady-state airflow from the mouth can be considered a limitation, however, it makes the simulations affordable from a computational point of view, compared to a full transient simulation, given the complexity of the mathematical model and the size of the three-dimensional domain. The approximation used to simulate a steady-state (constant) airflow from the mouth and then a transient droplet transport was widely used in the literature, as in (Arpino et al., 2023; Cortellessa et al., 2023; He et al., 2011; Li et al., 2021; Mirzaie et al., 2021; Seepana & Lai, 2012; van Beest et al., 2022). The temperature of the exhaled air was set at 35 °C (Arpino, Cortellessa, et al., 2022).

The Boundary Conditions (BCs) employed to solve the governing equations are reported in Table 2.

Table 2
BCs and the relative OpenFOAM BC functions (in italic) employed.

Physical quantity	Inlets	Outlets	Walls	Humans
u	Diffuser: volumetric airflow and rotatory motion (Table 1); *swirlFlowRateInletVelocity*; Mouth: volumetric airflow (0.66 l s^{-1}); *flowRateInletVelocity*	Outflow; *zeroGradient*	No-slip; *noSlip*	No-slip; *noSlip*
T	Diffuser: imposed temperature (Table 1); *fixedValue*; Mouth: imposed temperature (35 °C); *fixedValue*	Outflow; *zeroGradient*	Adiabatic; *zeroGradient*	Imposed temperature (33 °C); *fixedValue*
p_{rgh}	Inflow; *fixedFluxPressure*	Imposed value of 0 Pa; *fixedValue 0*	No outflow; *fixedFluxPressure*	No outflow; *fixedFluxPressure*
p	Calculated; *calculated*	Calculated; *calculated*	Calculated; *calculated*	Calculated; *calculated*
k	Derived value; *turbulentIntensityKineticEnergyInlet*	Outflow; *zeroGradient*	Wall function; *kLowReWallFunction*	Wall function; *kLowReWallFunction*
ε	Derived value; *turbulentMixingLengthDissipationRateInlet*	Outflow; *zeroGradient*	Wall function; *epsilonWallFunction*	Wall function; *epsilonWallFunction*
ν_t	Calculated; *calculated*	Calculated; *calculated*	Wall function; *nutKWallFunction*	Wall function; *nutKWallFunction*
α_t	Imposed value; *fixedValue*	Outflow; *zeroGradient*	Wall function; *compressible::alphatWallFunction*	Wall function; *compressible::alphatWallFunction*

In Table 2 *inlets* are the diffusers and the professor's mouth, *outlets* are the extraction grilles, *humans* are the students and the professor, *walls* are all the surfaces not belonging to other groups. u (m s^{-1}) is the air velocity, T (°C) is the temperature, p_{rgh} (Pa) is the pressure p minus the hydrostatic pressure (OpenCFD Ltd, 2018), k (J kg^{-1}) is the turbulent kinetic energy, ε (J kg^{-1} s^{-1}) is the turbulent kinetic energy dissipation, ν_t (m^2 s^{-1}) is the turbulent kinematic viscosity and α_t (m^2 s^{-1}) is the turbulent thermal diffusivity. When not specified in Table 2, the inlet BCs for diffusers and mouth are the same. The UC is adjacent to other air-conditioned rooms, except for a part on the ceiling equipped with the latest generation windows and blinds, therefore all the boundaries were considered adiabatic. This hypothesis can be considered effective for this kind of analysis, as proven and used in the literature (Arpino et al., 2023; D'Alicandro & Mauro, 2023b; Liu, Yin, et al., 2021a; Su et al., 2022). The BC employed for k and ε, respectively, calculate the inlet value from the user-supplied turbulent intensity (10%) and turbulent mixing length (7% of the inlet characteristic length). The *lowReCorrection* was implemented in the *epsilonWallFunction*. In OpenFOAM environment, the BC *calculated* means that the value is assigned via field assignment and not imposed as a BC value. The OpenFOAM solver *potentialFoam* was used to initialize the velocity field to improve the convergence and reduce the computational time.

3.2. Droplet transport model

The droplet transport model is based on a two-phase approach where there is the fluid and continuous phase (air) and the solid and discrete phase (droplets). The simulation is based on the hypothesis that the air velocity field influences the motion of the droplets while they do not modify air velocity, meaning that there is a one-way coupling between the fluid and the solid phase. Due to this hypothesis, droplet transport can evolve on a steady-state fluid velocity field. The motion of each droplet is calculated independently from the other droplets and the interaction between particles (collisions) is treated as fully elastic and droplet coagulation is not present. Furthermore, when a droplet settles on a surface, it can no longer be resuspended in air. The droplets were simulated spherically with a density (ρ_d) of 1 g cm^{-3} (Johnson et al., 2011).

The Lagrangian Particle Tracking (LPT) equations are employed to solve the Lagrangian phase (droplet motion). Among different forces acting on the droplets, only drag and gravity forces are considered, while the others can be neglected, according to van Beest et al. (van Beest et al., 2022). The LPT equations are reported in equations 6 and 7 (Arpino, Cortellessa, et al., 2022; Arpino et al., 2023; Cortellessa et al., 2021; van Beest et al., 2022; M. Wang, Lin, & Chen, 2012; Zhang & Chen, 2006):

$$\frac{dx_d}{dt} = u_d \tag{6}$$

$$m_d \frac{du_d}{dt} = F_D + F_g \tag{7}$$

where m_d (kg) is the droplet mass; u_d (m s^{-1}) is the droplet velocity; F_D (N) and F_g (N) are, respectively, the drag and gravity forces acting on the droplet and x_d (m) is the trajectory of the droplet. The drag force is calculated employing the equation 8-10 (Arpino, Cortellessa, et al., 2022; Arpino et al., 2023; Cortellessa et al., 2021; van Beest et al., 2022):

$$F_D = m_d \frac{18}{\rho_d d_d^2} C_D \frac{Re_d (u - u_d)}{24} \tag{8}$$

Table 3
Post-evaporation particle ($dC_n/dlog\ (d_d)$) concentration distributions fitted by five size ranges as adopted in the droplet transport simulations for speaking activity.

Expiratory activity	Post-evaporation	
	Particle diameter (size range), d_d (μm)	$dC_n/dlog\ (d_d)$ (part. cm^{-3})
speaking	1.0 μm (0.1–1.0 μm)	0.266
	1.9 μm (1.0–3.8 μm)	0.035
	5.0 μm (3.8–6.6 μm)	0.013
	9.8 μm (6.6–14.7 μm)	0.016
	16.8 μm (14.7–20.0 μm)	0.015

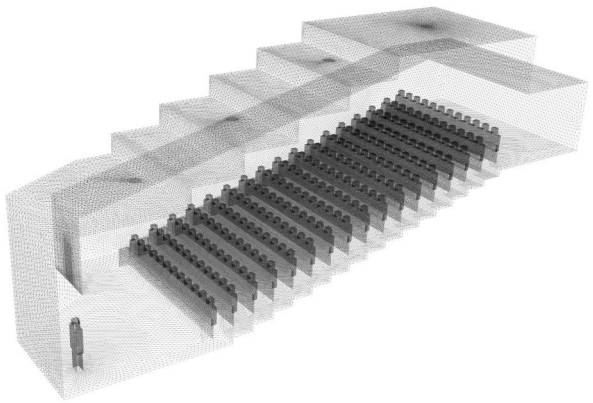

Fig. 2. Mesh (Mesh#2 8,109,714 elements) employed to perform the numerical simulation for case 3 and used as a prototype for the other meshes.

Table 4
Inlet velocity condition and mean values of the magnitude velocity and turbulent quantities in the UC, for all the simulated cases.

Cases	Inlet		Mean value in the UC			
	Vertical velocity (m s^{-1}) (z component)	Magnitude velocity range (m s^{-1})	Magnitude velocity (m s^{-1})	I (%) turbulent intensity	k (J kg^{-1}) turbulent kinetic energy	ε (J kg^{-1} s^{-1}) turbulent kinetic energy dissipation
Case 1: 6000 m^3 h^{-1}, 408 students	1.65	1.65–2.04	0.128	29.0	0.00264	0.00085
Case 2: 8000 m^3 h^{-1}, 408 students	2.21	2.21–2.73	0.156	29.1	0.00325	0.00147
Case 3: 10,000 m^3 h^{-1}, 408 students	2.76	2.76–3.41	0.181	28.3	0.00471	0.00236
Case 4: 10,000 m^3 h^{-1}, 204 students	2.76	2.76–3.41	0.166	30.3	0.00408	0.00219
Case 5: 10,000 m^3 h^{-1}, 0 students	2.76	2.76–3.41	0.150	29.5	0.00398	0.00187

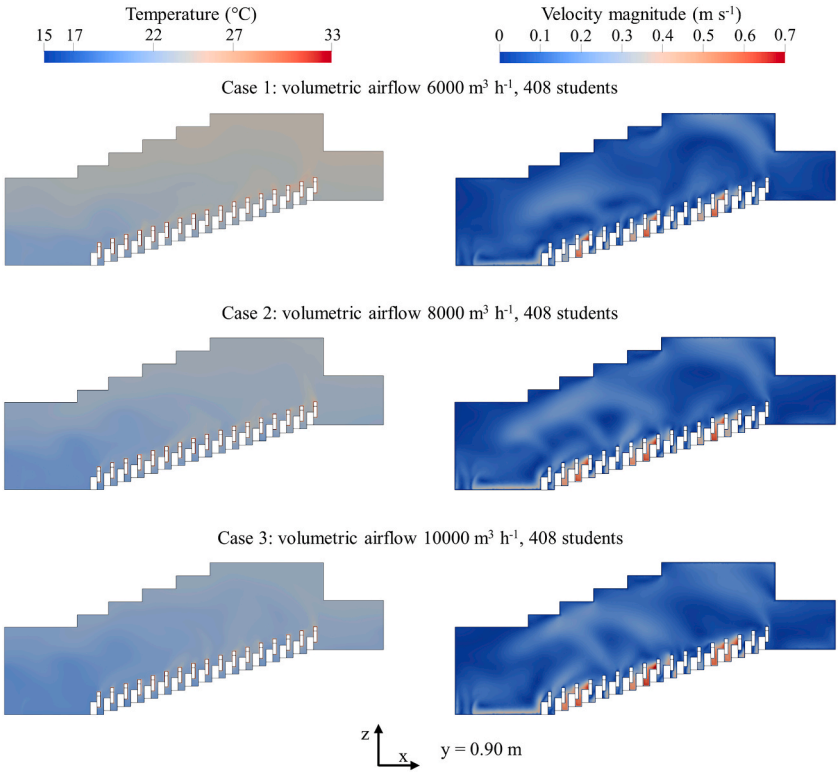

Fig. 3. Temperature and velocity magnitude distribution at the distance y = 0.90 from the symmetry plane, for the three different volumetric airflow (6000, 8000 and 10,000 $m^3\ h^{-1}$) at the full capacity (408 students).

$$Re_d = \frac{\rho(|u - u_d|)d_d}{\mu} \tag{9}$$

$$C_D = \begin{cases} \dfrac{24}{Re_d} \ \ if\ Re_d < 1 \\ \dfrac{24}{Re_d}\left(1 + 0.15\, Re_d^{0.687}\right) \ if\ 1 \le Re_d \le 1000 \\ 0.44\ if\ Re_d > 1000 \end{cases} \tag{10}$$

where: d_d (m) is the droplet diameter; C_D is the droplet drag coefficient; Re_d is the droplet Reynolds number. The LPT method is employable if the particle Stokes number, *Stk*, is lower than 0.1, which means that the particles mostly follow the airflow instead of settling very fast. This assumption is valid for the droplets simulated (Arpino et al., 2023).

The diameters (d_d) and relative concentrations (C_n) of the droplets emitted by the professor during the speaking activity were estimated from the experimental data provided by Johnson et al. (Johnson et al., 2011) and Morawska et al. (Morawska et al., 2009). They measured the number distribution of the particles in the range 0.5–1000 μm in close proximity to the mouth of an adult person while speaking. To calculate the final droplet concentration as a function of diameter, two hypotheses were considered: i) the liquid droplets evaporate in a very short time and distance (Balachandar et al., 2020; Cortellessa et al., 2021; Morawska et al., 2009; Xie et al., 2007), therefore directly the diameters post-evaporation were implemented in the model and further evaporation was not simulated, ii) particles with a diameter larger than 20 μm settle very fast and in a short distance from the source (Johnson et al., 2011), therefore they were not simulated.

The post-evaporation diameters were calculated from the pre-evaporation diameter employing equation 11 (Balachandar et al., 2020):

$$d_{post-ev} = d_{pre-ev}\, \psi^{\frac{1}{3}} \tag{11}$$

where $d_{post\text{-}ev}$ (μm) and $d_{pre\text{-}ev}$ (μm) are, respectively, the post- and pre-evaporation droplet diameter and ψ is the non-volatile (e.g. SARS-Cov-2 virus) percentage composition of the droplet, which is equal to ≈1% for the droplets exhaled from the mouth, resulting in a post-evaporation diameter equal to 0.215 times the pre-evaporation diameter. The direction of a single droplet is random inside a

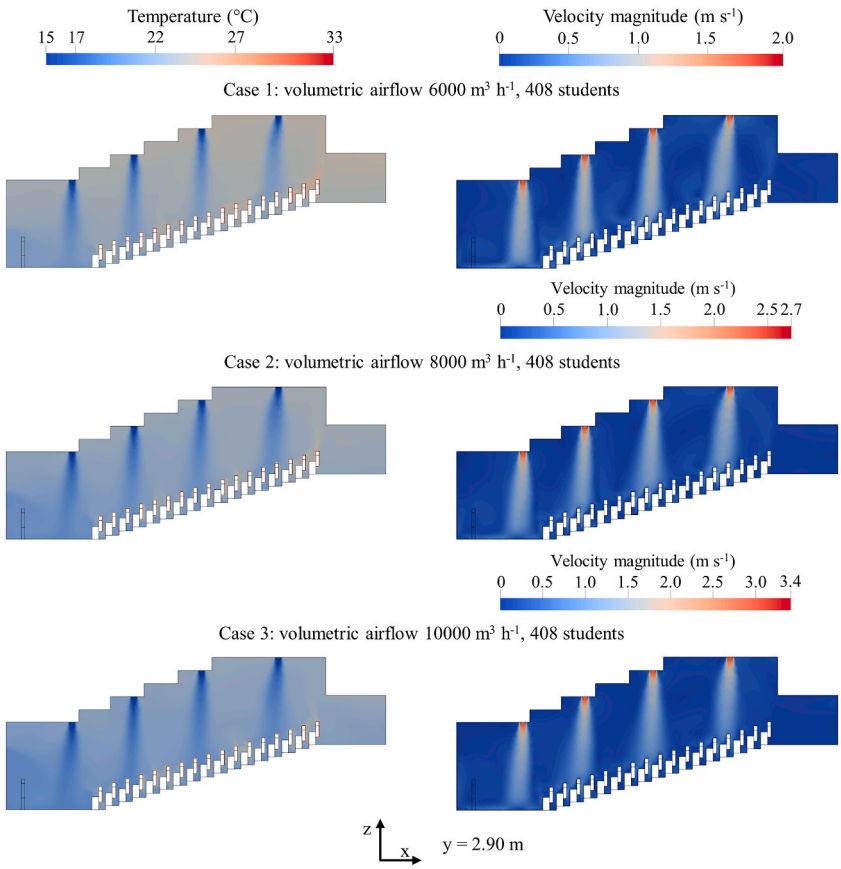

Fig. 4. Temperature and velocity magnitude distribution at the distance y = 2.90 from the symmetry plane, which is the plane where the diffusers are placed, for the three different volumetric airflow (6000, 8000 and 10,000 $m^3\ h^{-1}$) at the full capacity (408 students).

cone with an angle of 22°, as it was measured experimentally (Abkarian et al., 2020).

The original distribution, after the post-evaporation shrinking, was fitted through simplified distributions made up of five size ranges. The post-evaporation particle and volume concentration distributions for speaking activity in the function of the five diameter ranges used to model the droplet emission model in the simulations are summarized in Table 3.

During a lesson, the professor in most cases is not in a fixed position but moves near the blackboard. For this reason, the professor was not modelled in the middle of the symmetry plane but at a distance of 1 m from it. This implies, that there are two sources of droplets because the professor is duplicated, therefore only half droplet emission was imposed as BC to the professor's mouth, to have a global emission equal to one person split into two points (one for each professor model) to reproduce the non-static source position. The droplet concentration in the air entering the UC from the diffuser is 0 part. cm^{-3} because both the external air and the recirculated air pass through a fine filter (E12) that filters >99.5% of the particles with a diameter larger than 0.3 μm (European Norm, 2019). Therefore, the inflow air can be considered clean. The BCs employed for the droplet transport simulations are *rebound* for the symmetry plane to correctly simulate the symmetry and *escape* for the extraction grilles and walls to simulate the droplet evacuation through the outlet and deposition on surfaces. A *rebound* BC was used for the diffusers and mouth too, even if it is redundant because there is an inflow that avoids the droplet exit from those surfaces. The *gradientDispersionRAS* dispersion model was employed to correctly account for the turbulent effect on the aerosol transport.

3.3. Grid sensitivity analysis, discretization and convergence criteria

In order to ensure the adequate accuracy of the numerical results and to reduce the computational time, a grid sensitivity analysis was performed. Due to the complex geometry, second-order tetrahedral elements were employed to create unstructured meshes for all cases considered in the present work. The near wall mesh was modelled with 3 boundary layers. The OpenFOAM function *checkMesh* was used to check the quality indicators and the relative threshold for the meshes. To ensure a good quality of the grids, only meshes that satisfied these quality indicators were accepted for the grid sensitivity analysis. The following quality indicators and threshold values were checked: max non-orthogonality smaller than 70, mean non-orthogonality smaller than 20, max skewness smaller than 3 and max aspect ratio smaller than 10.

The grid sensitivity analysis was performed for the mesh at fully occupancy rate and airflow of 10,000 $m^3\ h^{-1}$ (case 3 in Table 1). It

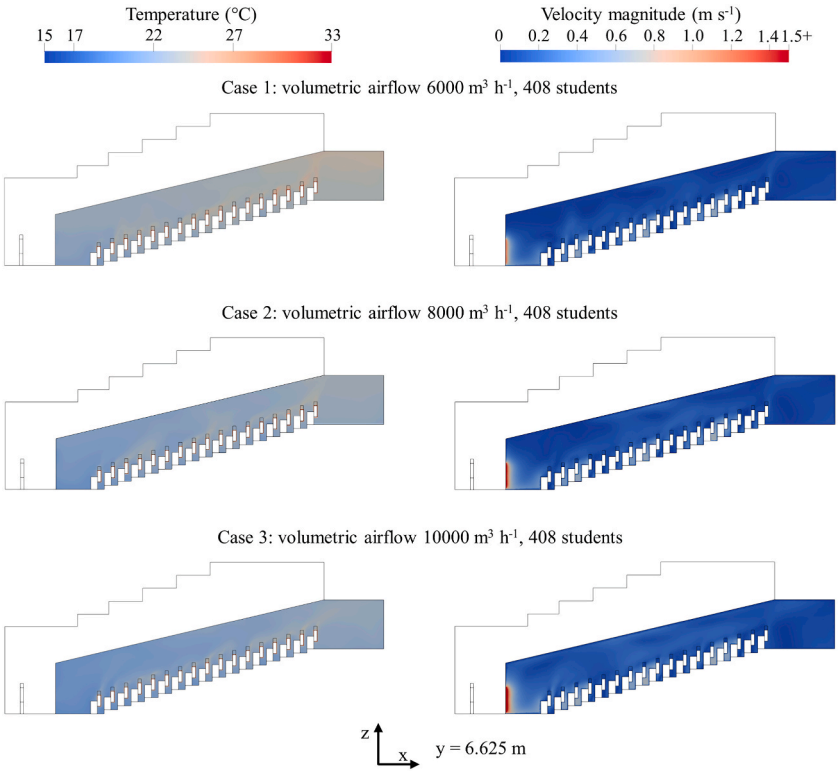

Fig. 5. Temperature and velocity magnitude distribution at the distance y = 6.625 from the symmetry plane, which is the plane where the extraction grille is placed, for the three different volumetric airflow (6000, 8000 and 10,000 $m^3\ h^{-1}$) at the full capacity (408 students).

was performed by comparing the magnitude velocity in the points at the perpendicular distance of 0.5 m from each diffuser. These points were chosen because the velocity is larger than in other internal points and they are at an adequate distance from the inlet, ensuring a good sensitivity in the results and a smoothed dependence on the inlet BC.

The four meshes created for the grid sensitivity analysis have a number of cells of 5,047,265 (mesh#1), 8,109,714 (mesh#2), 12,376,019 (mesh#3) and 17,146,418 (mesh#4). The velocity difference was compared at four points at 0.5 m from each diffuser, obtaining the following results: the difference between mesh#1 and mesh#4 is in the range of 2.9–8.4%, while between mesh#2 and mesh#4 is in the range of 0.3–1.1%, while between mesh#3 and mesh#4 is in the range of 0.1–0.3%; therefore mesh#2 was selected because it guarantees an excellent compromise between the independency of the results by the computational grid and computational time required for simulations. Mesh #2 has a max non-orthogonality of 62.18, mean non-orthogonality of 16.26, max skewness of 0.86 and max aspect ratio of 6.96. The first boundary layer has a y + value between 0.33 and 9.07, with an average value of 1.83. The meshes employed for the other cases with different occupancy rates were created employing the same parameters used for the mesh tested. The mesh chosen for full occupancy rate after the grid sensitivity analysis is represented in Fig. 2.

In both thermofluid dynamics and droplet transport simulations, the discretized equations were solved with the Geometric Algebraic MultiGrid (GAMG) method in conjunction with the Gauss–Seidel solver. A second-order upwind scheme was implemented to discretize the convective terms, while a second-order central difference scheme was implemented to discretize the diffusion terms and gradients. The Euler discretization was used for the time schemes in the transient droplet transport simulations. The droplet transport simulations were performed with a mean Courant number lower than 1 to improve the accuracy, the maximum Courant number, depending on the volumetric airflow, is between 10 and 20 (corresponding to a time step of the order of magnitude of 0.001 s). It is important to notice that the cells with higher Courant numbers are near the diffusers where the droplets do not arrive, therefore there is not a decrease of accuracy even with a maximum Courant number higher than 1.

Three criteria were used to assess the convergence: the reduction of the normalized residual of at least three orders of magnitude for all the quantities, the achievement of equality of inflow and outflow, the achievement of a constant value (between the SIMPLE pseudo-step) of the velocity magnitude at the points used for the grid sensitivity analysis.

4. Results and discussion

4.1. Thermofluid dynamics conditions

The vertical velocity and magnitude at the inlet (diffuser) and the mean values (averaged over the entire domain) of magnitude

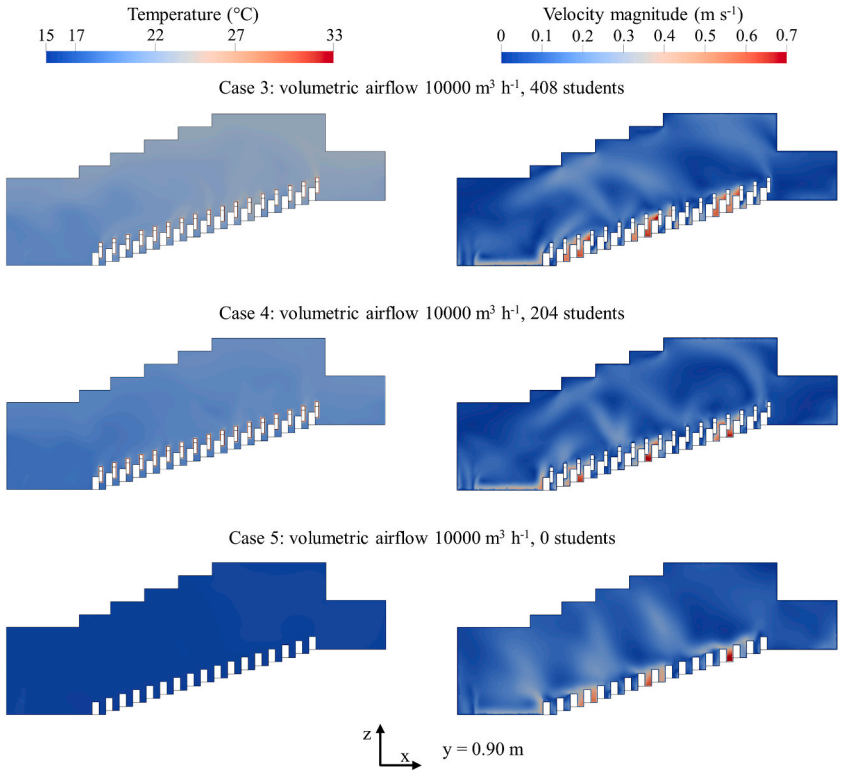

Fig. 6. Temperature and velocity magnitude distribution at the distance y = 0.90 from the symmetry plane, for the three different occupancy rates (408 students, 204 students and 0 students) at the volumetric airflow of 10,000 $m^3\ h^{-1}$.

velocity and turbulent quantities (k, ε, I) in the UC are reported in Table 4. The mean values were calculated using the *IntegrateVariable* function in ParaView.

The mean magnitude velocity, k, and ε, are an increasing function of the inlet velocity and thermal plume effect, that depends on the number of students. Instead, the turbulent intensity (I) is not proportional to these values and the variation between cases is very low. Analysing cases 3–5 it can be estimated that the presence of each 204 students increases the mean magnitude value of ≈16% due to the thermal plume.

The planes x-z are the most characteristic because x is the larger direction and the airflow mostly evolves in the z-direction, moreover, these planes can easily contain the professor, the students and the inlet or outlet. Therefore, the thermofluid dynamics conditions (temperature and velocity magnitude) calculated from the numerical simulations considering different volumetric flow rates (at full occupancy rate) are represented in three x-z planes at y = 0.90 m from the symmetry plane (Fig. 3), passing through the middle of the diffusers, at y = 2.90 m (Fig. 4), and the middle of the extraction grille, at y = 6.625 m (Fig. 5). While, the same images in the function of the occupancy rate (at a volumetric airflow of 10,000 $m^3\ h^{-1}$) are represented in Fig. 6 (y = 0.90 m), Fig. 7 (y = 2.90 m) and Fig. 8 (Y = 6.625 m). The figures and graphs were generated using ParaView and MatLab.

In the plane containing the diffusers (y = 2.90 m), which is shown in Figs. 4 and 7, the temperature between the diffusers increases with the decrease of the volumetric airflow due to the increase in the prevalence of the thermal plume. Moreover, as expected, the temperature difference decreases with a lower occupancy rate. From a qualitative point of view, the magnitude velocity is the same but the quantitative values are proportional to the volumetric airflow (Fig. 4); the difference in this plane is negligible by changing the occupancy rate (Fig. 7). This result is coherent with another work that studied the thermal plume with different inlet velocities in an operating room (D'Alicandro & Mauro, 2023a), where with high air velocity the thermal plume effect resulted negligibly. The effect of the thermal plume can be observed in the other two planes analysed (y = 0.90 m and y = 6.625 m) (Figs. 3, Figure 5, Figure 6, Figure 8) where the mean velocity is lower and, therefore, the buoyancy force generated by thermal plume has an increasing effect. The magnitude velocity is proportional to the occupancy rate because the effect of buoyancy is added to the air velocity, resulting in the creation of large-scale vortexes that cause recirculation flows. For case 5 which has 0 students and, therefore, with no thermal plume effect, the large-scale vortexes are not created. For all cases at the end of the UC behind the students (x > 21 m) where there is neither inlet nor outlet the magnitude air velocity is very low, creating a stagnation zone. As expected, the mean temperature is directly proportional to the occupancy rate and inversely proportional to the volumetric airflow, and the highest temperature is in the highest zone of the UC. This effect is appreciated during cold periods because warm air is trapped in the UC, but during hot periods it can be detrimental. To solve this, extraction grilles, that work only during hot periods, could be installed on the ceiling or in the upper part of the UC. Case 5 (empty UC) is not isothermal because the professor is present and there is a heat inflow from both the body temperature

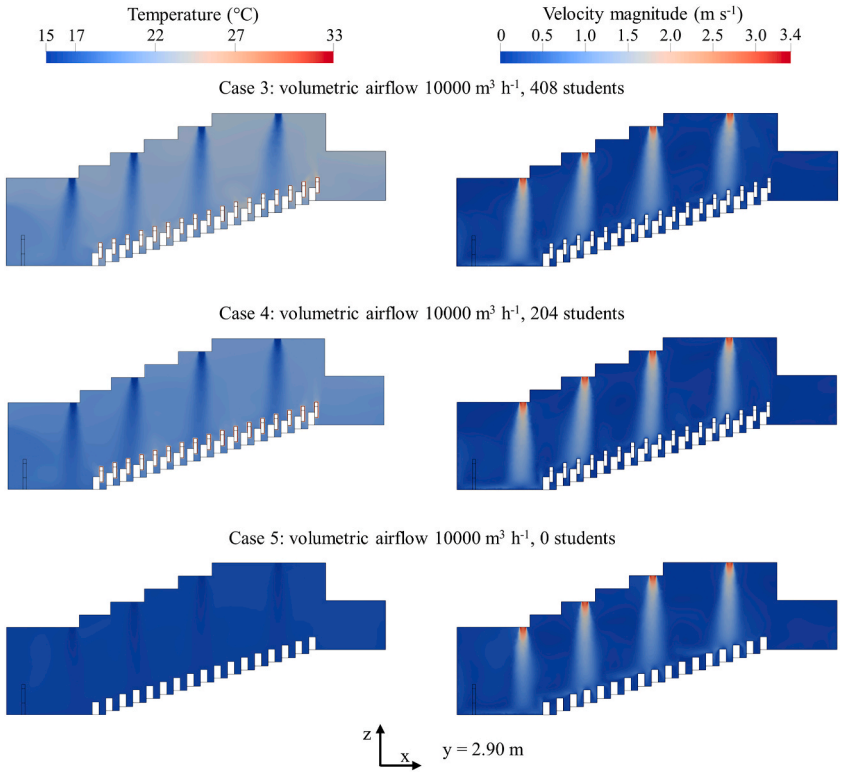

Fig. 7. Temperature and velocity magnitude distribution at the distance y = 2.90 from the symmetry plane, which is the plane where the diffusers are placed, for the three different occupancy rates (408 students, 204 students and 0 students) at the volumetric airflow of 10,000 m^3 h^{-1}.

and exhaled air.

The streamlines from the professor's mouth, droplet sources, influence the droplet transport and they are worth to be analysed. The streamlines are represented in Fig. 9. In case 5 which has no large-scale vortexes, the streamlines travel for longer along the UC before exiting through the extraction grille or ending when the velocity reaches a value close to 0. For this case a high droplet concentration along all the UC is expected. In case 4 there is a peculiar interaction between the inlet airflow and the thermal plume. This interaction generates a shield effect and all the streamlines go directly to the extraction grille without moving across the UC, therefore, it is expected that most of the droplets quickly evacuate the UC or settle in the zone between the professor and the first desk row. In cases 1–3, a higher concentration near the professor is expected with fewer droplets that are transported along the UC. In particular, for case 3 the droplet concentration should be higher near the floor.

4.2. *Droplets transport*

One of the most important aspect to be investigated about the droplet transport, is the fate of the droplets. This means calculating, in post-processing, how many droplets settle on surfaces, are evacuated by the HVAC system or remain suspended in the air. On the base of these results, considerations can be made about the concentration, dimension and age of the suspended droplets. The percentage of droplets settled on surfaces (professor, students and other surfaces such as walls and desks), evacuated or still suspended in the air are reported in Table 5. The percentage distribution of droplets as a function of the age and diameter, at the end of the simulation (t = 3600 s), are shown in Figs. 10 and 11. While their spatial distribution is reported in Figs. 12 and 13.

The percentage of droplets evacuated by the HVAC system is between 64% and 73% for all cases, except for case 5 which is 53%. This latter value is higher than the percentage of droplets evacuated reported in (Arpino et al., 2023), which is between 3% and 12%, due to the location of the extraction grilles that are placed in the upper part of the UC. Moreover, in two other works of some of the authors of the present paper, which simulated ultrafine particle transport in operating rooms, the evacuation rate was between 75% and 95% (D'Alicandro & Mauro, 2022; 2023a). This means that the HVAC system of the present UC effectively evacuates the droplets and other aerosol contaminants. Case 5 in addition to a higher deposition rate has a higher quantity of droplets still suspended in the air (12.31%) than the other cases, as shown from the analysis of the thermofluid dynamic condition. The reason is the absence of the thermal plume and the consequent not creation of large-scale vortexes. The second case with the highest quantity of droplets still suspended in the air is case 3 (10,000 m^3 h^{-1}, 408 students) with 6.61% compared to cases with lower volumetric airflow, case 1 (4.54%) and case 2 (3.76%), in absolute value is 1.46–1.76 times more droplets and their age is higher too (Fig. 10). From the point of view of air contamination, increasing volumetric airflow is not always beneficial, as demonstrated in (Arpino et al., 2023). This is a

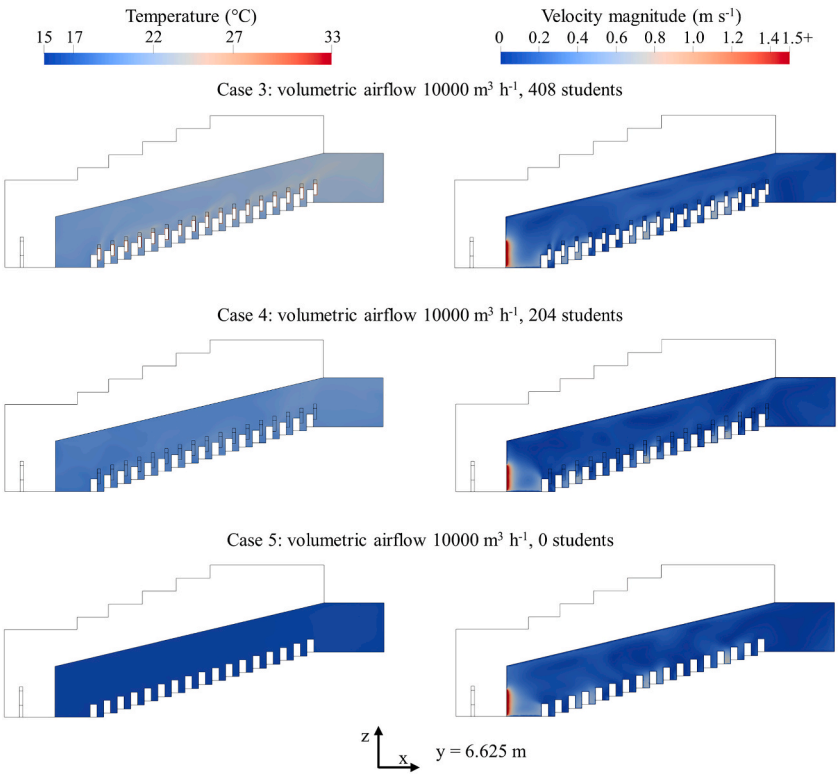

Fig. 8. Temperature and velocity magnitude distribution at the distance y = 6.625 from the symmetry plane, which is the plane where the extraction grille is placed, for the three different occupancy rates (408 students, 204 students and 0 students) at the volumetric airflow of 10,000 $m^3\ h^{-1}$.

reason why CFD simulations are needed to analyse different cases and scenarios and find the best or optimal configuration and working conditions of the HVAC system and quantify the coupling effects (i.e., with thermal plume).

Droplet age is the time the droplet was suspended in the air since its generation. Droplet generation occurred throughout all the simulation time (from t = 0 s to t = 3600 s), therefore some droplets are expected to have an age of a few seconds. In Fig. 10 the droplet ages are grouped in a range time of 300 s each, and the distribution percentage is an inverse function of the age. For cases 1, 2 and 4 the percentage of droplets with an age greater than 900 s is less than 10%, therefore 900 s (15 min) can be used as the cleaning time between two different lessons to drastically lower the contaminant concentration and improve the indoor air quality. For case 3, which has the highest volumetric airflow and occupancy rate, the cleaning time is double (1800 s), which is too long to be implemented. For all cases, after 5 min (300 s) the droplet concentration is at least halved, which is a good trade-off between cleaning time and UC use efficiency (reduction of idle time).

For each diameter, the percentage of droplets still suspended in the air relative to the number of droplets generated is around 10% with no significant difference as a function of diameter, so even the droplets with the largest diameter (16.8 μm) remain suspended in the air for a time comparable to that of the droplets with the smallest diameter (1 μm). This result is consistent with data from the literature (Johnson et al., 2011; Morawska et al., 2009; Xie et al., 2007). The difference is in the number of droplets generated for each diameter, the number of particles generated with a diameter of 1 μm is higher than other diameters (Table 3). This is reflected in the droplets distribution as a function of the diameter: ≈85% of the droplet suspended in the air (at t = 3600 s) have a diameter of 1 μm and there is no significant difference in the distribution between the simulated cases (Fig. 11). The spatial distribution of the droplet in the function of the diameter is almost uniform, with no accumulation or lack of droplets with a certain diameter in a certain zone of the UC (Fig. 13). This means that the airflow pattern has a low influence on the fate of the droplets as a function of their diameter. As a result, only one droplet diameter can be simulated to reduce the complexity of the numerical model.

A result from the previous analysis of the streamlines and the magnitude velocity field, is that the interaction between the inlet airflow and the buoyancy effect creates a large-scale vortex, which can strongly influence the droplet concentration and their fate within the UC. This analysis can be combined with the analysis of the spatial distribution of the droplets (Figs. 12 and 13). There is a direct correlation between the streamlines coverage and the droplet distribution within the UC. In fact, in case 5, where the streamlines cover almost the entire UC, the droplets are distributed along the entire UC, with a lower concentration under the diffusers due to the inlet airflow. In this case, as expected, the droplet age increases with distance from the source, in the area on the opposite side with respect to the professor position, the droplet age is between 400 and 600 s for most of the droplets; this means that the even if the droplets reach the end of the UC they do not stay in that zone for a long time, but they settle or return and evacuate through the

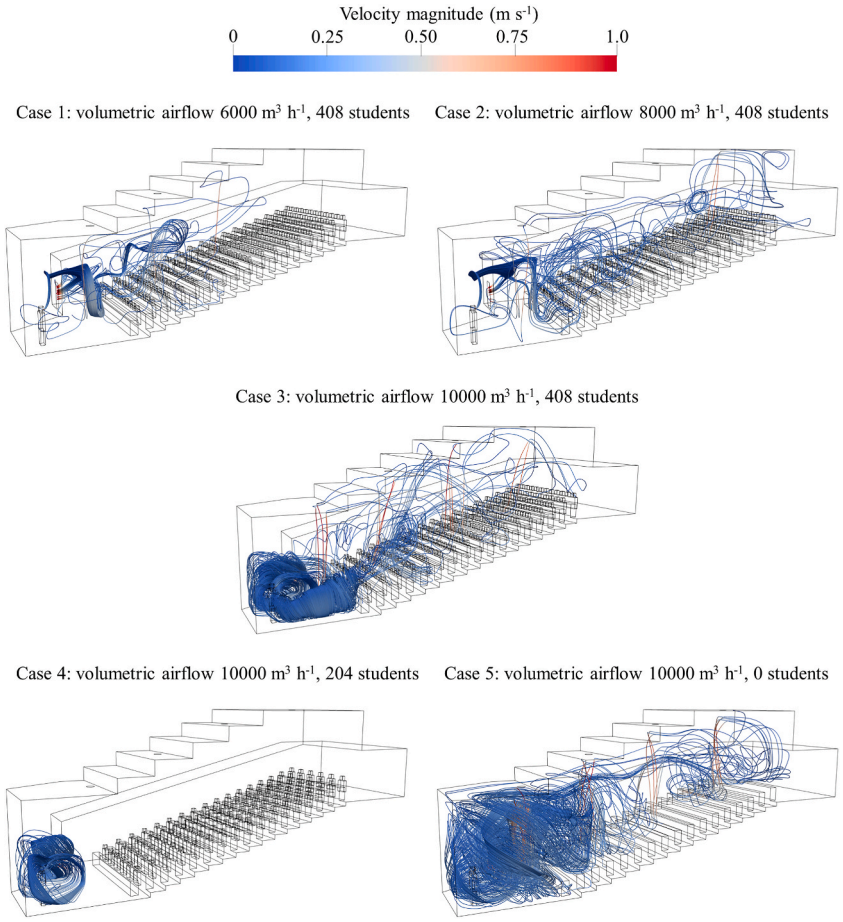

Fig. 9. The streamlines generated from professor's mouth (droplet source) for all the simulated cases.

Table 5
The percentage of droplets settled on surfaces (professor, students and other surfaces such as walls and desks), evacuated or still suspended in the air, for all the simulated cases.

Case	Droplet settled on			Droplet evacuated	Droplet suspended in the air
	Professor	Students	Walls and desks		
Case 1: 6000 m^3 h^{-1}, 408 students	9.26%	2.29%	18.96%	64.95%	4.54%
Case 2: 8000 m^3 h^{-1}, 408 students	8.48%	2.40%	17.13%	68.23%	3.76%
Case 3: 10,000 m^3 h^{-1}, 408 students	10.70%	2.27%	8.89%	71.53%	6.61%
Case 4: 10,000 m^3 h^{-1}, 204 students	11.56%	1.33%	9.04%	73.63%	4.44%
Case 5: 10,000 m^3 h^{-1}, 0 students	10.25%	n.a.	24.15%	53.29%	12.31%

extraction grille. Considering that the deposition rate for case 5 is higher, most of the droplets settle along the entire UC, infecting all desks. Instead, for the other cases the droplet passing through the first desk row are lower, for case 4 they are much lower, due to the fact that all the streamlines go toward the extraction grille.

In this configuration for all cases, the main direction of the airflow is vertical and in the highest zone of the UC there is a high concentration of droplets and a fraction of them will move toward the rows of desks farthest from the source; therefore, the use of physical barriers between the source and the desks has a negligible impact on the contamination because the droplets pass over the barriers. The barriers have more effect if the main direction of the airflow is horizontal (Abuhegazy et al., 2020; Mirzaie et al., 2021). Behind the professor there is an accumulation of droplets because there are walls that trap them and, in particular, near the ceiling, there is a stagnation zone (except in case 5). Installing another extraction grille can be a solution to this problem, but the airflow patterns and droplet transport must be simulated again because they can be substantially changed by the installation of the extraction grille. The installation or opening of a window is not the optimal solution because the airflow is difficult to be predicted, considering that it depends on the atmospheric condition.

Case 5 demonstrates how important it is to consider occupant-generated heat (thermal plume) in both thermofluid dynamics and

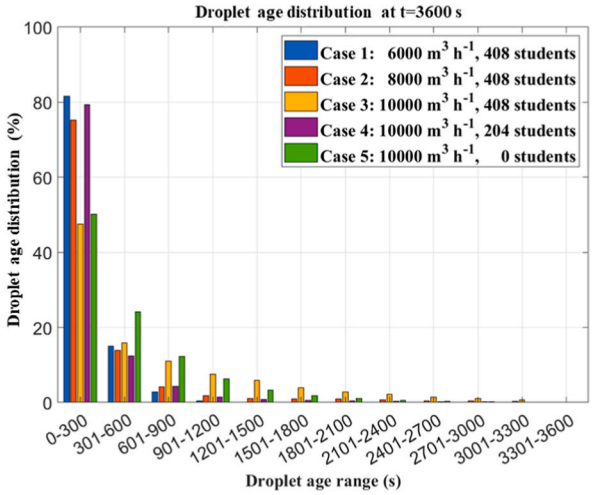

Fig. 10. Droplet distribution as function of the age range, at the end of simulation (t = 3600 s), for all the simulated cases.

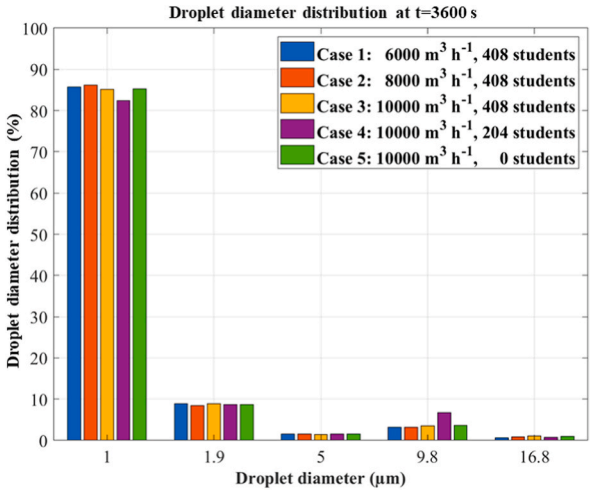

Fig. 11. Droplet distribution as function of the diameter, at the end of simulation (t = 3600 s), for all the simulated cases.

droplet transport simulations. Ignoring the thermal plume can lead to completely different results. In any case, the thermal plume depends on the number of occupants and their location so it is difficult to establish it a priori or to perform simulations that cover all the most probable cases, as there would be too many of them. Moreover, the effect of the volumetric airflow and occupancy rate on the thermofluid dynamics condition and droplet transport is not linear, therefore, when analysing a case, it is important to perform several simulations by varying some key parameters, to have a general behaviour within the indoor environment. Help can come from machine learning algorithms, which by taking a large amount of simulations as input can quickly draw conclusions or parameterize the simulations.

5. Conclusions

In this work, the thermofluid dynamic conditions and the droplet transport were numerically simulated inside a real large University Classroom (UC), as a function of the occupancy rate and the inlet volumetric airflow rate. To decouple the effects of the Heating, Ventilation and Air Conditioning (HVAC) system inlet conditions and the thermal plume generated by humans, the simulations were divided into two groups. In the first group, the UC occupancy rate was maintained at its maximum (408 students) and three different inlet volumetric airflows were simulated: 10,000 $m^3\ h^{-1}$, 8000 $m^3\ h^{-1}$ and 6000 $m^3\ h^{-1}$. This group of simulations has allowed to analyse the effects of the inlet airflow, while maintaining constant the internal heat sources. In the second group, three different occupancy rates were considered, keeping constant the inlet airflow: full occupancy, which is the design condition of the UC; half occupancy, which can be considered as a condition to ensure social distancing; empty UC, to have a term of comparison for the study of droplets transport and airflow inside the room. This second group of simulations has allowed to analyse the effects of the thermal

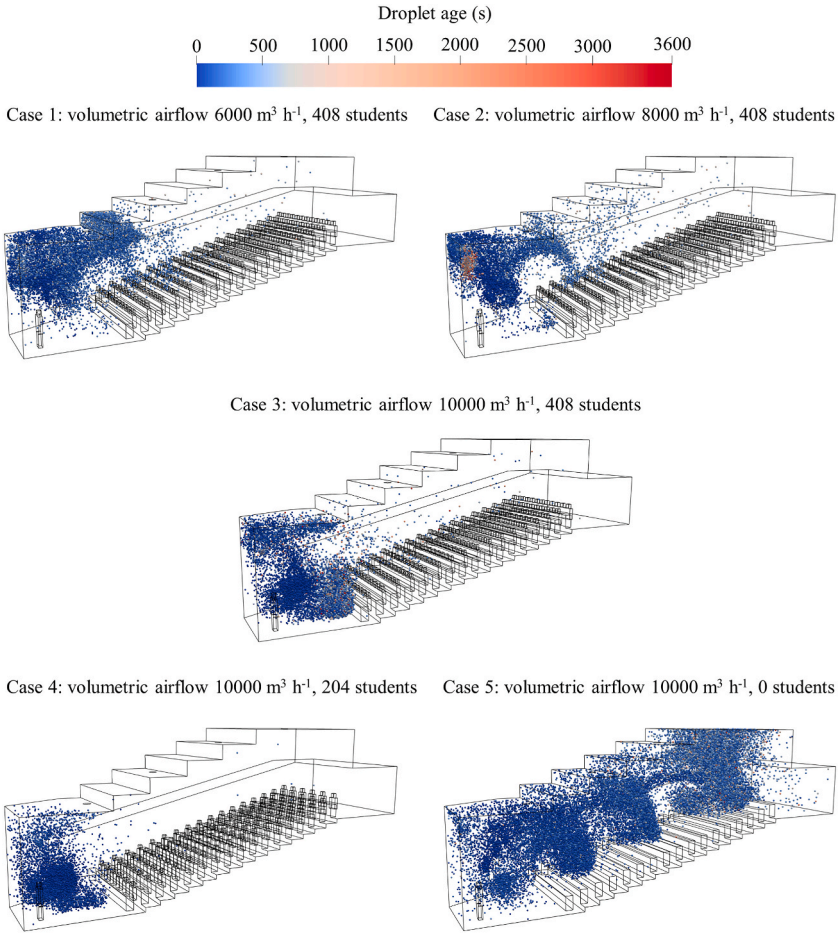

Fig. 12. Droplet spatial distribution represented by the age, at the end of the simulation (t = 3600 s) for all the simulated cases.

plume on the indoor airflow pattern.

OpenFOAM was used to perform the numerical simulations. The thermofluid dynamic conditions were reproduced employing a steady-state, turbulent and compressible, solver based on the SIMPLE algorithm, and employing the Boussinesq approximation for the buoyancy effects. The droplet transport, divided into five size groups in a range between 1 and 16.8 μm, was simulated by solving the Lagrangian Particle Tracking (LPT) equations.

The main results obtained can be summarized as follows.

1. The thermal plume brings an increase of the mean magnitude velocity by a factor of about 16% for every 204 students (half occupancy rate). The quantities k and ε also increase due to the thermal plume, while I is not affected. The thermal plume effect is negligible in the plane containing the diffusers (inlet plane), where the mean magnitude velocity is larger with respect to the other planes where the velocity is lower;
2. The thermal plume (generated by the buoyancy forces due to the presence of a significant number of students), combined with the inlet airflow, creates large-scale vortexes, that cause recirculation flows. In fact, for case 5 (10,000 $m^3\,h^{-1}$, 0 students), the thermal plume is not present and, as a consequence, the large-scale vortexes are not generated;
3. The streamlines derived from the professor's mouth, i.e. droplet source, influence the droplet transport and they are worth to be analysed. In particular, in case 5 (10,000 $m^3\,h^{-1}$, 0 students), where no large-scale vortexes are observed, the streamlines are longer and travel along the UC, increasing the risk of droplet contamination. In case 4 (10,000 $m^3\,h^{-1}$, 204 students) there is a peculiar interaction between the inlet airflow and the thermal plume, that generates a shield effect. As a consequence, all the streamlines are concentrated near the extraction grille, without moving across the UC, reducing the risk of contamination in the UC;
4. The HVAC system installed in the UC effectively evacuates the droplets and other aerosol contaminants in the presence of a significant occupancy rate, obtaining a percentage of evacuation between 53.29% and 73.63%;
5. Case 3 (10,000 $m^3\,h^{-1}$, 408 students) is characterized by a quantity of droplets suspended in the air of 6.61%, larger with respect to cases with lower volumetric airflow (between 3.76% and 4.54%), and their age is larger too. This proves that increasing inlet volumetric airflow is not always beneficial for the reduction of aerosol contamination, while the air distribution inside indoor

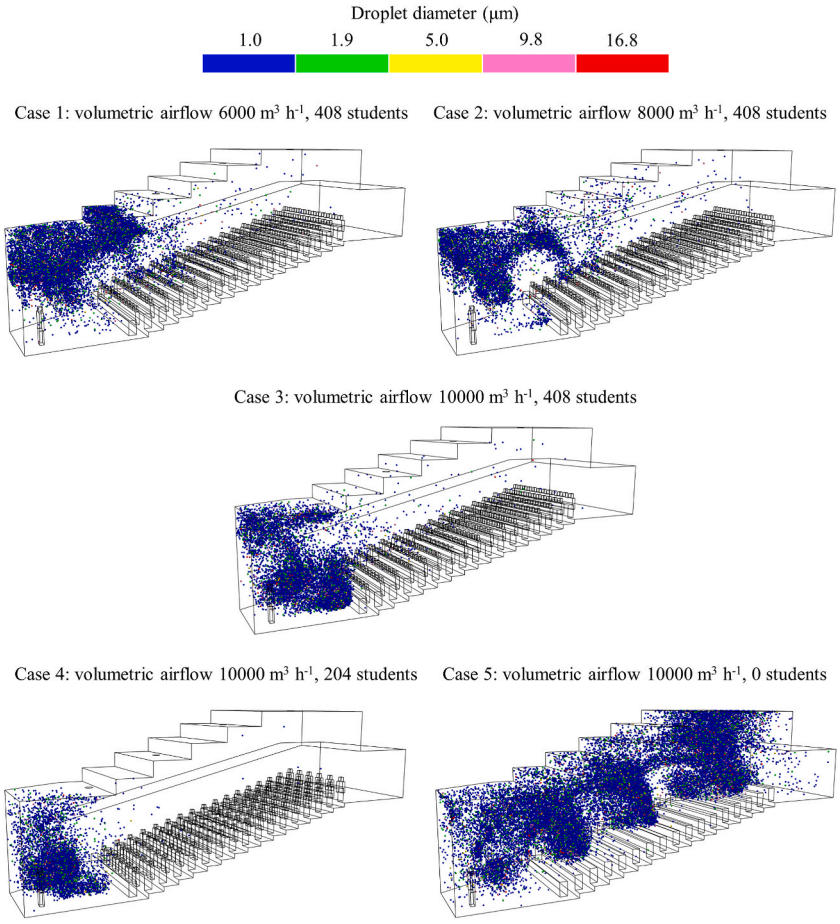

Fig. 13. Droplet spatial distribution represented by the diameter, at the end of the simulation (t = 3600 s) for all the simulated cases.

environments assumes a crucial role. This is a reason why Computational Fluid Dynamics (CFD) simulations are needed to analyse different cases and scenarios in the design stage, find the optimal configuration and working conditions of the HVAC system, and quantify the coupling effects;

6. For all the simulated cases, after 5 min (600 s) the droplet concentration is at least halved, while for 3 cases (1, 2 and 4) after 15 min (900 s) the droplet concentration is less than 10%; therefore at least 5 min should be considered as a trade-off value for the cleaning time between two successive lectures;
7. The UC is an indoor environment characterized by turbulence with non-stagnant air velocity. For all the simulated cases, the percentage of droplets suspended in the air and their spatial distribution has very low dependence on their diameter (for diameter values between 1 and 16.8 μm). As a result, only one droplet diameter can be simulated in order to simplify the numerical model;
8. If the main direction of the airflow is vertical, the use of physical barriers can have a negligible effect on airborne transmission, as it is in the case analysed, because the droplets pass over the barriers.

Declaration of competing interest

The authors declare that they have no known competing financial interests or personal relationships that could have appeared to influence the work reported in this paper.

Data availability

Data will be made available on request.

Acknowledgements

The authors gratefully acknowledge the financial support of project PRIN 2020 "Optimal refurbishment design and management of small energy micro-grids - OPTIMISM", Prot. 20204NXSZH, CUP I65F21001850006, Ministero dell'Università e della Ricerca (MUR).

References

Abkarian, M., Mendez, S., Xue, N., Yang, F., & Stone, H. A. (2020). Speech can produce jet-like transport relevant to asymptomatic spreading of virus. *Proceedings of the National Academy of Sciences of the United States of America, 117*(41), 25237–25245. https://doi.org/10.1073/pnas.2012156117

Abuhegazy, M., Talaat, K., Anderoglu, O., Poroseva, S. V., & Talaat, K. (2020). Numerical investigation of aerosol transport in a classroom with relevance to COVID-19. *Physics of Fluids, 32*(10). https://doi.org/10.1063/5.0029118

Arjmandi, H., Amini, R., khani, F., & Fallahpour, M. (2022). Minimizing the respiratory pathogen transmission: Numerical study and multi-objective optimization of ventilation systems in a classroom. *Thermal Science and Engineering Progress, 28*. https://doi.org/10.1016/j.tsep.2021.101052

Arpino, F., Cortellessa, G., D'Alicandro, A. C., Grossi, G., Massarotti, N., & Mauro, A. (2023). CFD analysis of the air supply rate influence on the aerosol dispersion in a university lecture room. *Building and Environment, 235*, Article 110257. https://doi.org/10.1016/j.buildenv.2023.110257

Arpino, F., Cortellessa, G., Grossi, G., & Nagano, H. (2022). A Eulerian-Lagrangian approach for the non-isothermal and transient CFD analysis of the aerosol airborne dispersion in a car cabin. *Building and Environment, 209*, Article 108648. https://doi.org/10.1016/j.buildenv.2021.108648. November 2021.

Arpino, F., Grossi, G., Cortellessa, G., Mikszewski, A., Morawska, L., Buonanno, G., et al. (2022). Risk of SARS-CoV-2 in a car cabin assessed through 3D CFD simulations. *Indoor Air, 32*(3). https://doi.org/10.1111/ina.13012

Balachandar, S., Zaleski, S., Soldati, A., Ahmadi, G., & Bourouiba, L. (2020). Host-to-host airborne transmission as a multiphase flow problem for science-based social distance guidelines. *International Journal of Multiphase Flow, 132*, Article 103439. https://doi.org/10.1016/j.ijmultiphaseflow.2020.103439

van Beest, M. R. R. S., Arpino, F., Hlinka, O., Sauret, E., van Beest, N. R. T. P., Humphries, R. S., et al. (2022). Influence of indoor airflow on particle spread of a single breath and cough in enclosures: Does opening a window really 'help'. *Atmospheric Pollution Research, 13*(7), Article 101473. https://doi.org/10.1016/j.apr.2022.101473

Benchetrit, G., Shea, S. A., Pham Dinh, T., Bodocco, S., Baconnier, P., & Guz, A. (1989). Individuality of breathing patterns in adults assessed over time. *Respiration Physiology, 75*.

Buonanno, G., Robotto, A., Brizio, E., Morawska, L., Civra, A., Corino, F., et al. (2022). Link between SARS-CoV-2 emissions and airborne concentrations: Closing the gap in understanding. *Journal of Hazardous Materials*. https://doi.org/10.1016/j.jhazmat.2022.128279

Cardelli, R., Puglisi, G., Su, R., Ferrari, S., Bl, T., & Mazzarella, L. (2022). *Ventilation strategies to reduce airborne transmission of viruses in classrooms : A systematic review of scientific literature air Change per hour* (Vol. 222). https://doi.org/10.1016/j.buildenv.2022.109366. March.

Caretto, L. S., Gosman, A. D., Patankar, S. V., & Spalding, D. B. (2007). Two calculation procedures for steady, three-dimensional flows with recirculation. In *Proceedings of the third international conference on numerical methods in fluid mechanics*. https://doi.org/10.1007/bfb0112677

Chen, Q. (1995). COMPARISON OF DIFFERENT k-ε MODELS FOR INDOOR AIR FLOW COMPUTATIONS. *Numerical Heat Transfer, Part B: Fundamentals: An International Journal of Computation and Methodology, 28*(3), 353–369.

Chin, J. (2000). *Control of communicable diseases manual*. Disease Control.

Chow, T. T., Lin, Z., & Bai, W. (2006). The integrated effect of medical lamp position and diffuser discharge velocity on ultra-clean ventilation performance in an operating theatre. *Indoor and Built Environment, 15*(4), 315–331. https://doi.org/10.1177/1420326X06067802

Cortellessa, G., Canale, C., Stabile, L., Grossi, G., Buonanno, G., & Arpino, F. (2023). Effectiveness of a portable personal air cleaner in reducing the airborne transmission of respiratory pathogens. *Building and Environment, 235*, Article 110222. https://doi.org/10.1016/j.buildenv.2023.110222. January.

Cortellessa, G., Stabile, L., Arpino, F., Faleiros, D. E., van den Bos, W., Morawska, L., et al. (2021). Close proximity risk assessment for SARS-CoV-2 infection. *Science of the Total Environment, 794*, Article 148749. https://doi.org/10.1016/j.scitotenv.2021.148749

Dacunto, P., Moser, D., Ng, A., & Benson, M. (2022). Classroom aerosol dispersion: Desk spacing and divider impacts. *International journal of Environmental Science and Technology, 19*(2), 1057–1070. https://doi.org/10.1007/s13762-021-03564-z

D'Alicandro, A. C., Massarotti, N., & Mauro, A. (2021). Aerosol hazards in operating rooms: A review of numerical and experimental studies. *Journal of Aerosol Science, 158*, Article 105823. https://doi.org/10.1016/j.jaerosci.2021.105823. June.

D'Alicandro, A. C., & Mauro, A. (2022). *Effects of operating room layout and ventilation system on ultrafine particle transport and deposition* (Vol. 270). Atmospheric Environment. https://doi.org/10.1016/j.atmosenv.2021.118901

D'Alicandro, A. C., & Mauro, A. (2023a). Air change per hour and inlet area: Effects on ultrafine particle concentration and thermal comfort in an operating room. *Journal of Aerosol Science, 171*, Article 106183. https://doi.org/10.1016/j.jaerosci.2023.106183

D'Alicandro, A. C., & Mauro, A. (2023b). Experimental and numerical analysis of CO2 transport inside a university classroom: Effects of turbulent models. *Journal of Building Performance Simulation*. https://doi.org/10.1080/19401493.2022.2163423

Ding, E., Zhang, D., & Bluyssen, P. M. (2022). Ventilation regimes of school classrooms against airborne transmission of infectious respiratory droplets: A review. *Building and Environment, 207*(PA), Article 108484. https://doi.org/10.1016/j.buildenv.2021.108484

European Norm. (2019). *EN 1822-1:2019 High efficiency air filters (EPA, HEPA and ULPA) - Part 1: Classification, performance testing, marking*.

Fiala, D., Lomas, K. J., & Stohrer, M. (1999). A computer model of human thermoregulation for a wide range of environmental conditions: The passive system. *Journal of Applied Physiology*. https://doi.org/10.1152/jappl.1999.87.5.1957

Foster, A., & Kinzel, M. (2021). Estimating COVID-19 exposure in a classroom setting: A comparison between mathematical and numerical models. *Physics of Fluids, 33*(2). https://doi.org/10.1063/5.0040755

Gao, X., Li, Y., & Leung, G. M. (2009). *Ventilation control of indoor transmission of airborne diseases in an Urban community*. *Indoor and Built Environment*. https://doi.org/10.1177/1420326X09104141

Guo, M., Xu, P., Xiao, T., He, R., Dai, M., & Miller, S. L. (2021). Review and comparison of HVAC operation guidelines in different countries during the COVID-19 pandemic. *Building and Environment, 187*(4800), Article 107368. https://doi.org/10.1016/j.buildenv.2020.107368

Gupta, J. K., Lin, C. H., & Chen, Q. (2009). Flow dynamics and characterization of a cough. *Indoor Air, 19*(6), 517–525. https://doi.org/10.1111/j.1600-0668.2009.00619.x

Gupta, J. K., Lin, C. H., & Chen, Q. (2010). Characterizing exhaled airflow from breathing and talking. *Indoor Air, 20*(1), 31–39. https://doi.org/10.1111/j.1600-0668.2009.00623.x

He, Q., Niu, J., Gao, N., Zhu, T., & Wu, J. (2011). CFD study of exhaled droplet transmission between occupants under different ventilation strategies in a typical office room. *Building and Environment, 46*(2), 397–408. https://doi.org/10.1016/j.buildenv.2010.08.003

International Organization for Standardization. (2005). *ISO 7730:2005 Ergonomics of the thermal environment - analytical determination and interpretation of thermal comfort using calculation of the PMV and PPD indices and local thermal comfort criteria*.

Isukapalli, S. S., Mazumdar, S., George, P., Wei, B., Jones, B., & Weisel, C. P. (2013). Computational fluid dynamics modeling of transport and deposition of pesticides in an aircraft cabin. *Atmospheric Environment, 68*, 198–207. https://doi.org/10.1016/j.atmosenv.2012.11.019

Johnson, G. R., Morawska, L., Ristovski, Z. D., Hargreaves, M., Mengersen, K., Chao, C. Y. H., et al. (2011). Modality of human expired aerosol size distributions. *Journal of Aerosol Science*. https://doi.org/10.1016/j.jaerosci.2011.07.009

Kwon, S. B., Park, J., Jang, J., Cho, Y., Park, D. S., Kim, C., et al. (2012). Study on the initial velocity distribution of exhaled air from coughing and speaking. *Chemosphere, 87*(11), 1260–1264. https://doi.org/10.1016/j.chemosphere.2012.01.032

Li, W., Chong, A., Hasama, T., Xu, L., Lasternas, B., Tham, K. W., et al. (2021). Effects of ceiling fans on airborne transmission in an air-conditioned space. *Building and Environment, 198*, Article 107887. https://doi.org/10.1016/j.buildenv.2021.107887. January.

Liu, Z., Yin, D., Niu, Y., Cao, G., Liu, H., & Wang, L. (2021a). Effect of human thermal plume and ventilation interaction on bacteria-carrying particles diffusion in operating room microenvironment. *Energy and Buildings, 254*, Article 111573. https://doi.org/10.1016/j.enbuild.2021.111573

Liu, Z., Zhang, M., Cao, G., Tang, S., Liu, H., & Wang, L. (2021b). Influence of air supply velocity and room temperature conditions on bioaerosols distribution in a class I operating room. *Building and Environment, 204*, Article 108116. https://doi.org/10.1016/j.buildenv.2021.108116. May.

Mahjoub Mohammed Merghani, K., Sagot, B., Gehin, E., Da, G., & Motzkus, C. (2021). A review on the applied techniques of exhaled airflow and droplets characterization. *Indoor Air, 31*(1), 7–25. https://doi.org/10.1111/ina.12770

Massarotti, N., Mauro, A., Mohamed, S., Nowak, A. J., & Sainas, D. (2020). Fluid dynamic and thermal comfort analysis in an actual operating room with unidirectional airflow system. *Building Simulation, 14*(4), 1127–1146. https://doi.org/10.1007/s12273-020-0713-3

Massarotti, N., Mauro, A., Sainas, D., Marinetti, S., & Rossetti, A. (2019). A novel procedure for validation of flow simulations in operating theaters. *Science and Technology for the Built Environment, 25*(5), 629–642. https://doi.org/10.1080/23744731.2018.1556053

Mirzaie, M., Lakzian, E., Khan, A., Warkiani, M. E., Mahian, O., & Ahmadi, G. (2021). COVID-19 spread in a classroom equipped with partition – a CFD approach. *Journal of Hazardous Materials, 420*, Article 126587. https://doi.org/10.1016/j.jhazmat.2021.126587. June.

Morawska, L., & Cao, J. (2020). Airborne transmission of SARS-CoV-2: The world should face the reality. In *Environment international*. https://doi.org/10.1016/j.envint.2020.105730

Morawska, L., Johnson, G. R., Ristovski, Z. D., Hargreaves, M., Mengersen, K., Corbett, S., et al. (2009). Size distribution and sites of origin of droplets expelled from the human respiratory tract during expiratory activities. *Journal of Aerosol Science, 40*(3), 256–269. https://doi.org/10.1016/j.jaerosci.2008.11.002

Nicas, M., Nazaroff, W. W., & Hubbard, A. (2005). Toward understanding the risk of secondary airborne infection: Emission of respirable pathogens. *Journal of Occupational and Environmental Hygiene, 2*(3), 143–154. https://doi.org/10.1080/15459620590918466

OpenCFD Ltd. (2018). Hydrostatic pressure effects. https://www.openfoam.com/documentation/guides/latest/doc/guide-applications-solvers-variable-transform-p-rgh.html.

Pope, S. B. (2000). *Turbulent flows*. Cambridge University Press.

Rencken, G. K., Rutherford, E. K., Ghanta, N., Kongoletos, J., & Glicksman, L. (2021). Patterns of SARS-CoV-2 aerosol spread in typical classrooms. *Building and Environment, 204*, Article 108167. https://doi.org/10.1016/j.buildenv.2021.108167. April.

Ren, J., Wang, Y., Liu, Q., & Liu, Y. (2021). Numerical study of three ventilation strategies in a prefabricated COVID-19 inpatient ward. *Building and Environment, 188*, Article 107467. https://doi.org/10.1016/j.buildenv.2020.107467. July 2020.

Rohdin, P., & Moshfegh, B. (2007). Numerical predictions of indoor climate in large industrial premises. A comparison between different k-ε models supported by field measurements. *Building and Environment, 42*(11), 3872–3882. https://doi.org/10.1016/j.buildenv.2006.11.005

Seepana, S., & Lai, A. C. K. (2012). Experimental and numerical investigation of interpersonal exposure of sneezing in a full-scale chamber. *Aerosol Science and Technology, 46*(5), 485–493. https://doi.org/10.1080/02786826.2011.640365

Stavrakakis, G. M., Koukou, M. K., Vrachopoulos, M. G., & Markatos, N. C. (2008). Natural cross-ventilation in buildings: Building-scale experiments, numerical simulation and thermal comfort evaluation. *Energy and Buildings, 40*(9), 1666–1681. https://doi.org/10.1016/j.enbuild.2008.02.022

Su, W., Yang, B., Melikov, A., Liang, C., Lu, Y., Wang, F., et al. (2022). Infection probability under different air distribution patterns. *Building and Environment, 207* (PB), Article 108555. https://doi.org/10.1016/j.buildenv.2021.108555

Tian, Z. F., Tu, J. Y., Yeoh, G. H., & Yuen, R. K. K. (2006). On the numerical study of contaminant particle concentration in indoor airflow. *Building and Environment, 41* (11), 1504–1514. https://doi.org/10.1016/j.buildenv.2005.06.006

Versteeg, H. K., & Malalasekera, W. (2007). *An introduction to computational fluid dynamics* (2nd ed.). https://doi.org/10.1109/mcc.1998.736434 Person Education.

Wang, M., Lin, C. H., & Chen, Q. (2012). Advanced turbulence models for predicting particle transport in enclosed environments. *Building and Environment, 47*(1), 40–49. https://doi.org/10.1016/j.buildenv.2011.05.018

Wang, Y., Zhao, F. Y., Kuckelkorn, J., Liu, D., Liu, J., & Zhang, J. L. (2014). Classroom energy efficiency and air environment with displacement natural ventilation in a passive public school building. *Energy and Buildings, 70*, 258–270. https://doi.org/10.1016/j.enbuild.2013.11.071

Wilcox, D. C. (2006). *Turbulence modeling for CFD*. DCW Industries.

Xie, X., Li, Y., Chwang, A. T. Y., Ho, P. L., & Seto, W. H. (2007). How far droplets can move in indoor environments - revisiting the Wells evaporation-falling curve. *Indoor Air, 17*(3), 211–225. https://doi.org/10.1111/j.1600-0668.2007.00469.x

Xu, C., Nielsen, P. V., Liu, L., Jensen, R. L., & Gong, G. (2017). Human exhalation characterization with the aid of schlieren imaging technique. *Building and Environment, 112*, 190–199. https://doi.org/10.1016/j.buildenv.2016.11.032

Xu, G., & Wang, J. (2017). CFD modeling of particle dispersion and deposition coupled with particle dynamical models in a ventilated room. *Atmospheric Environment, 166*, 300–314. https://doi.org/10.1016/j.atmosenv.2017.07.027

Xu, S., Zhang, G., Liu, X., & Li, X. (2023). CFD modelling of infection control in indoor environments: A focus on room-level air recirculation systems. *Energy and Buildings, 288*, Article 113033. https://doi.org/10.1016/j.enbuild.2023.113033

Yakhot, V., Orszag, S. A., Thangam, S., Gatski, T. B., & Speziale, C. G. (1992). Development of turbulence models for shear flows by a double expansion technique. *Physics of Fluids, 4*(7), 1510–1520. https://doi.org/10.1063/1.858424

Yan, Y., Li, X., & Tu, J. (2019). Thermal effect of human body on cough droplets evaporation and dispersion in an enclosed space. *Building and Environment, 148*, 96–106. https://doi.org/10.1016/j.buildenv.2018.10.039. October 2018.

Zhang, Z., & Chen, Q. (2006). Experimental measurements and numerical simulations of particle transport and distribution in ventilated rooms. *Atmospheric Environment, 40*(18), 3396–3408. https://doi.org/10.1016/j.atmosenv.2006.01.014

Zhang, Y., Hui, F. K. P., Duffield, C., & Saeed, A. (2022). A review of facilities management interventions to mitigate respiratory infections in existing buildings. *Building and Environment, 221*, Article 109347. https://doi.org/10.1016/j.buildenv.2022.109347. March.

Zhao, B., Zhang, Y., Li, X., Yang, X., & Huang, D. (2004). Comparison of indoor aerosol particle concentration and deposition in different ventilated rooms by numerical method. *Building and Environment, 39*(1), 1–8. https://doi.org/10.1016/j.buildenv.2003.08.002